1. Unpulsed magnetospheric emission, and PWN searches

In this section, we will search for emission in the phase range between the peaks of the pulsar's light curve. This potential DC emission could originate in the pulsar winds, from inside a pulsar's magnetosphere, or the emission could be physically unrealted to the pulsar.

GeV emission in the off-peak regions around LAT-detected pulsars has been studied in several previous publications. In particular, the spatially-extended Vela X pulsar wind nebula has been detected by the LAT in the off-peak region of the Vela pulsar (Ackermann et al. 2011) and the Crab nebula has been detected by the LAT (Abdo et al. 2010b). Surprisingly, this GeV emission from the Crab nebula was found to be variable in time (Abdo et al. 2011).

Most prominently, a dedicated analysis was performed using LAT data of the off-peak emission of 54 LAT-detected pulsars using 16 months of survey observations (Ackermann et al. 2011). The search discovered ten pulsars with significant off-peak emission. Along with Vela X and the Crab nebula, the search discovered a source coincident with the TeV source HESS J1023-575 in the off-peak window of PSR J1023-5746. In addtion, five of the other regions showed a significantly cutoff pulsar-like spectrum and are suspected to be of magnetospheric origin.

We expand upon this previous work by searching in the off-peak region of all 117 pulsars in this catalog. In addition to the larger list of pulsars, we use an expanded observation time, a larger energy range, and an improved analysis method.

1.1. Off-peak Phase Selection

To study the off-peak emission of LAT-detected pulsars, we first developed a systematic method to define the off-peak region of a pulsar. The primary constraint for this method was for it to be systematic, model independent, and computationally efficient.

The method we developed proceeds by deconstructing the pulsar's phaseogram into simple Bayesian Blocks using the algorithm described in Jackson et al. (2005). To produce Bayesian Blocks on a periodic phaseogram, we applied the blocks three sets of the data from a phase of -1 to 2 and selected the blocks from a phase of 0 to 1.

TO improve the off-peak region definition, we first optimized the pulsar phaseogram by varying the minimum energy and radius of the included photons to optimize the H-test. We then selected the lowest block to be the off-peak region, but removed 10% of the emission from either side of the block to avoid potential contamination.

There is one free parameter in the Baysian Block algorithm called $\mathrm{ncp}_{\mathrm{prior}}$ which modifies the probability that the algorithm will divide a block into smaller intervals. For our situation, we found that setting $\mathrm{ncp}_{\mathrm{prior}} = 8$ protected against the Bayesian Block decomposition containing unphysically small blocks. For a few very marginally-detected pulsars, the algorithm failed decomposed the phaseogram into multiple blocks and in these situations we decreased $\mathrm{ncp}_{\mathrm{prior}}$ until the algorithm succeeded.

In some situations, there can be two well defined off-peak regions between two pulsed peaks. The method we used to select a second phase range was to take the second lowest Bayesian block but only when the emission in this block is consistent with the emission in the lowest block (at the 99% confidence level) and when the second block contained at least half as much phase as the first block.

Figure Figure 1 shows the energy-and-radius optimized light curve and the off-peak selection for a representative sample of pulsars. The off-peak definition for all pulsars is contained in the auxiliary material.

1.2. Off-peak Analysis Method

We developed a procedure for characterizing emission found in off-peak phase region for all pulsars in this catalog. This procedure used both the spectral and spatial characteristics of any observed emission to determine its physical origin.

PWNe are often expected to be spatially resolvable at GeV energies. For example, Vela X and HESS J1825-137 are PWN that have been spatially resolved by the LAT (Ackermann et al. 2011; Grondin et al. 2011). On the other hand, not all PWN are expected to be significantly spatially resolved due to the finite instrument resolution of the LAT. For example, the Crab nebula cannot be resolved by that LAT LAT but is distinguished from the Crab pulsar in the off-peak region by its hard spectrum for $\mathrm{E} \gtrsim 1$ GeV. (Abdo et al. 2010b).

On the other hand, pulsars can have DC emission in the off-peak region due to the geometry of the pulsar magnetospheres. A previous analysis by the LAT collaboration found five off-peak regions to have significant emission which is point-like in nature and characterized by a pulsar-like cutoff spectrum (Ackermann et al. 2011). We can therefore use either spatial extension or a hard spectrum to distinguish PWN emission and point-like emission with a cutoff spectrum to distinguish magnetospheric emission.

To perform this analysis, we used the likelihood fitting package `pointlike` to study the spatial character of emission in the off-peak regions and `gtlike` in binned model to study

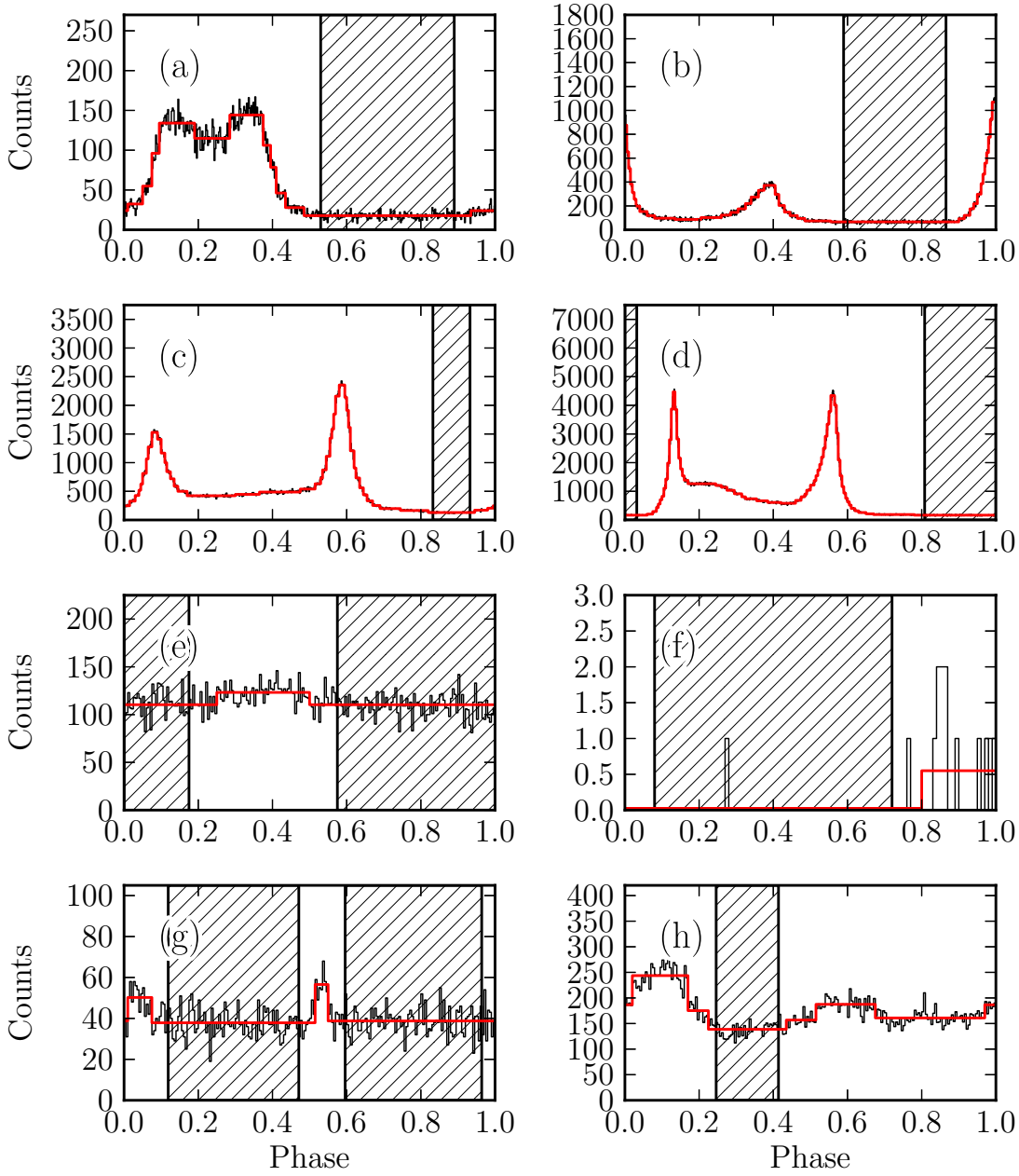

Fig. 1.— The phaseogram and off-peak selection for (a) PSRJ0007+7303, (b) PSRJ0534+2200, (c) PSRJ0633+1746, (d) PSRJ0835-4510, (e) PSRJ1702-4128, (f) PSRJ1747-4036, (g) PSRJ1801-2451, and (h) PSRJ2021+4026. The black histogram represents the energy-and-radius optimized phaseogram. The gray lines (colored red in the electronic version) represent the Bayesian block decomposition of the pulsar light curves. The hatched areas represent the off-peak regions selected by this method.

the spectral character of the emission. These tools provide complementary features and this method is very similar to the approach used in the second LAT catalog (Nolan et al. 2012) and a follow up search for spatially extended sources (Lande et al. 2012).

For this analysis, we build a model of the sky consistent with the second LAT catalog. We included as background sources all nearby sources from the second catalog and we also used the same background models (Nolan et al. 2012). For out analysis, we used an energy range from 100 MeV to 316 GeV ($10^{5.5}$ MeV). For this analysis, we removed all photons from the on-peak emission and scaled the exposure so as to fit the all-phase flux assuming the emission was constant with phase.

First, we assumed any potential emission in the off-peak region to have a point-like spatial model and (unless otherwise noted) a power-law spectral model. We used `pointlike` to fit the position of the off-peak region following the procedure described in Nolan et al. (2012). We used the best fit positions obtained by `pointlike` and performed a spectral analysis using `gtlike`.

With the best-fit position, we used `gtlike` to test the significance of the detection of the source. We define the likelihood-ratio test for the detection of the source as

$$\mathrm{TS} = 2\log(\mathcal{L}_{\mathrm{pt}}/\mathcal{L}_{\mathrm{bg}}) \tag{1}$$

where $\mathcal{L}_{\mathrm{pt}}$ is the Poisson likelihood for a model including the source and $\mathcal{L}_{\mathrm{bg}}$ the likelihood for a model not including the source. We set the threshold for detection of significant emission at $\mathrm{TS} > 25$, corresponding to a significance just over 4σ (Abdo et al. 2010a).

For the significantly-detected source, we tested to see if the spectrum of the source is significantly cutoff following the prescription in Ackermann et al. (2011). We fit the source in `gtlike` with both a power-law and exponentially-cutoff spectral model and define the likelihood-ratio test for a cutoff spectrum as

$$\mathrm{TS}_{\mathrm{cutoff}} = 2\log(\mathcal{L}_{\mathrm{cutoff}}/\mathcal{L}_{\mathrm{pt}}) \tag{2}$$

where $\mathcal{L}_{\mathrm{cutoff}}$ is the Poisson likelihood for a model including the cutoff spectrum. We set the threshold for detecting a significant cutoff at $\mathrm{TS}_{\mathrm{cutoff}} > 16$, corresponding to a 4σ detection (Ackermann et al. 2011) .

We used `pointlike` to simultaneously fit the position and the extension of the assumed radially-symmetric Gaussian source, following the description in (Lande et al. 2012). After the extension fit, we refit the spectrum of the spatially extended source using `gtlike` We tested the significance of the spatial extension and computed the likelihood-ratio test for the significance of the extension:

$$\mathrm{TS}_{\mathrm{ext}} = 2\log(\mathcal{L}_{\mathrm{ext}}/\mathcal{L}_{\mathrm{pt}}). \tag{3}$$

Here, $\mathcal{L}_{\rm ext}$ is the Poisson likelihood assuming the source is spatially extended. We set the threshold for detecting the significance of a spatially extended source at $\mathrm{TS}_{\rm ext} > 16$, corresponding to a 4σ detection (Lande et al. 2012).

The spectrum of the Crab nebula was uniquely challenging because the GeV spectrum contains both a falling synchrotron spectrum and an inverse component component (Abdo et al. 2010b). To avoid unnecessary complications in our pipeline, for this particular source we used the best fit two-component spectral model from Buehler et al. (2012) and fit only the overall normalization of the source.

For sources that are not significantly detected, we compute flux upper limits assuming a point-like spatial model and a fixed spectral index of 2.0. We also compute pulsed upper limit assuming a canonical pulsar spectrum with an index of -1.7 and a cutoff energy of 3 GeV.

To better assess the spectral charter of any emission in the off-peak region, we performed a spectral analysis in three independent energy bins (100 MeV to 1 GeV, 1 GeV to 10 GeV, and 10 GeV to 316 GeV). In each bin, we independently fit the flux and the spectral index of the source. We also computed flux upper limit assuming a fixed spectral index of 2 when the source was not significantly detected in the energy range.

Following the discovery of time-variable emission from the Crab nebula by the LAT, it is interesting to search for other variable PWN (Abdo et al. 2011). Therefore, we tested all off-peak regions for variability. We divided the 3-year time range into 36 month-long intervals and fit the flux of the source independently in each time range. We computed the significance of variability with a likelihood-ratio test by computing $\mathrm{TS}_{\rm var}$ following the procedure of 2FGL (Nolan et al. 2012). Since we divided our time range into 36 months-long bins, the null distribution for $\mathrm{TS}_{\rm var}$ follows a χ^2 distribution with 35 degrees of freedom. We set the detection criteria for significant variability at $\mathrm{TS}_{\rm var} > 91.7$, corresponding to a 4σ significance detection threshold.

In many situations, our pipeline was significantly biased due to systematic errors associated with not modeling nearby sources. We are more sensitive to nearby sources than the second LAT catalog both because of our expanded data set (3 years of observations instead of 2) and also because, for very bright pulsars, we are more sensitive to nearby sources once the strong contribution from the pulsar has been removed.

The large and energy dependent point-spread function of the LAT causes the analysis of any one source to be sensitively affected by the modeling of nearby sources. Therefore, we had to, in many situations, iteratively improve the model of a region by including new background sources. We modeled these sources by generating maps of residual test statistic

assuming the presence of a new source (of a fixed spectral index of 2) and looking for residuals with TS $\geq$ 25. In these situations, we would include a new source into our model, fit the position and spectrum of this source, and iterate until there was no remaining significant residual.

Even so, there are still some lingering regions for where we were unable to obtain an unbiased fit. the emission for. These issues are most likely due to systematics associated with the model of the galactic diffuse emission and issues associated with modeling nearby sources. The most common symptom of a failed fit is a diverging localization or an unphysically large extension which causes the source model to incorporate multiple background sources. Systematics associated with modeling extended sources are discussed more thoroughly in (Lande et al. 2012). For the currently analysis, we flagged these problematic regions and do not attempt a complete understanding of the region.

1.3. Results

After analyzing the off-peak emission using the pipeline described in § 1.2, we consider any emission in the off-peak region to be magnetospheric in nature if the emission is not significantly-extended and has a significantly-cutoff spectrum. We consider the emission to originate in the pulsar wind if it is spatially extended or had a hard spectral index. If the source is point-like and had a soft spectrum, or if it is formally spatially extended but if the best-fit extension is biased by nearby point-like sources, we flag the source as confused and do not speculate on the origin of the emission. For these confused regions, we include in our results the best fit spectrum at the position of the pulsar assuming a point-like spectral model.

A condensed summary of the results of the pipeline can be found in Table 1. This table includes the significance of the source, extension, and cutoff as well as the spectrum of the source. In addition, Figure **??** shows the best fit spectral models for a selection of the significantly-detected sources.

Consistent with (Abdo et al. 2011), we found the Crab nebula to be highly variable with TS_{var} =XXXXXX. Besides that, we found no significantly variable off-peak emission. The results of the variability test are contained in the auxiliary information.

The results of the spectral analysis in smaller energy bands described in section § **??** are included in the auxiliary information. In addition, upper limits computed assuming a power law spectral model and a canonical pulsar spectrum are included in the auxiliary information.

Table 1. Off-Peak Spatial and Spectral Results

PSR	Phase	TS_{point}	TS_{ext}	TS_{cutoff}	$F_{0.1-316}$ (10^{-9} erg cm^{-2} s^{-1})	Γ	E_{cutoff} (MeV)
J0007+7303	0.53 - 0.89	71.2	10.8	0.0	47.22 ± 8.60	2.61 ± 0.14	···
J0034−0534	0.21 - 0.68	42.8	0.0	4.9	16.82 ± 4.58	2.44 ± 0.16	···
J0101−6422	0.22 - 0.61	25.2	0.0	18.2	45.76 ± 6.41	-5.00 ± 0.00	100.02 ± 1.46
J0102+4839	0.81 - 0.57	69.6	0.0	5.3	26.34 ± 4.89	2.42 ± 0.10	···
J0106+4855	0.67 - 0.03, 0.18 - 0.54	25.5	0.0	0.2	29.14 ± 7.04	2.80 ± 0.17	···
J0218+4232	0.82 - 0.21	50.1	0.0	6.6	55.94 ± 11.20	2.72 ± 0.13	···
J0340+4130	0.13 - 0.64	26.8	0.1	16.5	2.45 ± 1.48	0.93 ± 2.51	645.30 ± 580.54
J0534+2200	0.59 - 0.87	5253.1	0.0	0.0	764.73 ± 18.42	···	···
J0633+1746	0.83 - 0.93	3649.0	2.3	237.3	719.12 ± 27.80	-1.42 ± 0.09	998.24 ± 116.74
J0734−1559	0.28 - 0.84	28.4	10.7	33.4	31.63 ± 6.36	1.77 ± 0.40	100.10 ± 3.01
J0835−4510	0.81 - 0.03	506.0	241.9	0.0	431.14 ± 22.25	2.11 ± 0.03	···
J0908−4913	0.66 - 0.04, 0.17 - 0.54	35.5	9.3	74.1	40.13 ± 37.59	-1.20 ± 0.71	999.01 ± 0.71
J1023−5746	0.67 - 0.03	84.8	57.7	14.1	230.75 ± 6722.99	2.04 ± 0.72	···
J1044−5737	0.55 - 0.97	27.9	187.0	0.0	243.05 ± 2.30	1.95 ± 0.00	···
J1105−6107	0.73 - 0.46	28.9	36.6	78.6	161.16 ± 6644.93	2.14 ± 0.72	···
J1112−6103	0.31 - 0.04	122.2	93.4	12.4	232.99 ± 26.43	2.12 ± 0.04	···
J1119−6127	0.59 - 0.18	40.7	18.3	0.0	54.59 ± 3399.22	2.16 ± 0.70	···
J1124−5916	0.69 - 0.05	86.2	0.0	24.2	26.39 ± 19.44	-0.79 ± 0.72	1000.00 ± 0.71
J1410−6132	0.55 - 0.24	42.4	91.6	12.5	81.41 ± 2783.70	1.79 ± 0.72	···
J1513−5908	0.53 - 0.15	100.6	2.1	0.0	15.83 ± 984.68	1.74 ± 0.72	···
J1620−4927	0.54 - 0.98	27.9	0.5	39.9	72.80 ± 22.94	-0.86 ± 0.25	1000.00 ± 173.04
J1744−1134	0.14 - 0.74	61.4	0.0	15.0	33.38 ± 15.81	2.25 ± 0.09	···
J1746−3239	0.41 - 0.99	53.8	7.2	42.0	61.29 ± 54.13	-1.18 ± 0.71	999.95 ± 0.71
J1747−2958	0.66 - 0.1	53.6	0.0	102.6	146.08 ± 125.15	-1.17 ± 0.71	991.64 ± 0.70
J1809−2332	0.53 - 0.91	31.5	13.0	15.2	85.80 ± 49.10	2.45 ± 0.11	···
J1813−1246	0.77 - 0.01	57.8	0.0	12.0	147.87 ± 33.22	2.46 ± 0.05	···
J1836+5925	0.76 - 0.92	10450.2	0.0	364.6	497.25 ± 10.72	-1.49 ± 0.02	2024.58 ± 59.89
J2021+4026	0.25 - 0.41	1712.8	37.4	228.3	1248.80 ± 20643.72	2.23 ± 0.72	···
J2043+1711	0.79 - 0.06, 0.18 - 0.55	151.6	0.0	11.9	23.36 ± 9.33	2.18 ± 0.08	···
J2055+2539	0.37 - 0.87	117.0	0.0	30.4	30.05 ± 31.95	-1.45 ± 0.70	999.99 ± 0.71
J2124−3358	0.09 - 0.69	177.7	0.0	27.0	10.88 ± 3.78	-0.61 ± 0.64	1000.01 ± 437.18
J2302+4442	0.75 - 0.23	113.7	0.0	8.4	34.35 ± 5.34	2.36 ± 0.09	···

Note. — A condensed version of the spectral analysis of sources detected significantly in the off-peak regions. This table includes the significance of the source, extension, and spectral cutoff (TS, TS_{ext}, TS_{cutoff}). The table also includes the best fit spectrum for these sources. For sources that are significantly cutoff, the spectral index and cutoff energy are from the fit of a cutoff spectrum.

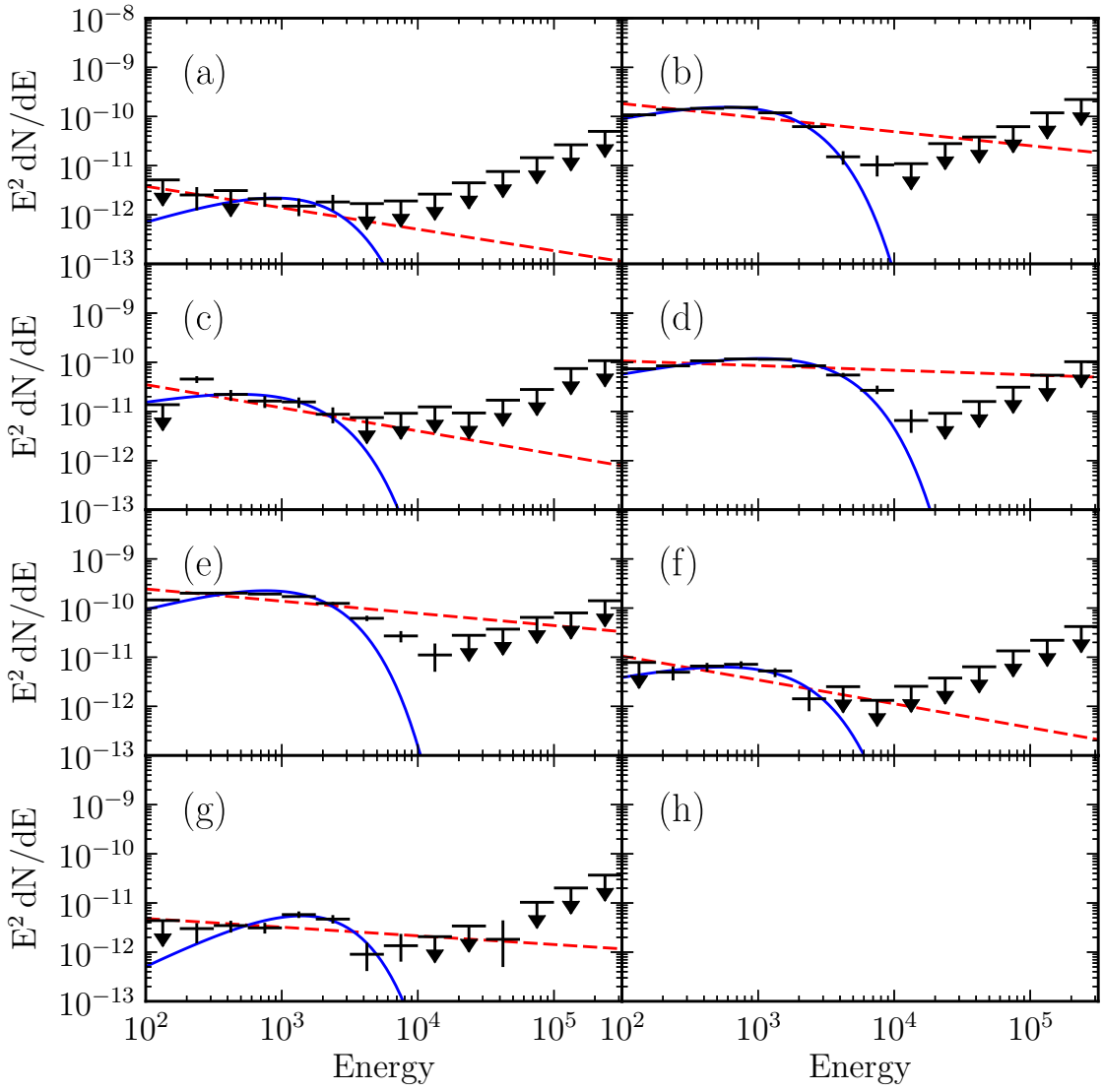

Fig. 2.— SEDs for several sources significantly-detected in the off-peak region.

In our pipeline, we found XXXXX off-peak regions to show significant PWNe. We detected the Vela X PWN (associated with PSRJ0835−4510), the Crab Nebula (associated with PSRJ0534+2200), and MSH 15−52 (associated with PSRJ1513-5908).

- What to say about PSRJ1023-5746, which was a PWN in PWNCAT1, but here shows a complicated spectrum???

We detected XXXXX of the regions to show clear magnetopsheric pulsar emission. These pulsars are ...

And Finally, we found XXXXX regions which where the analysis could not decisively determine the nature of the emission.

- PSRJ0101-6422 was fit to have an unphysically soft spectrum. We suspect that source is an artifact of problems modeling the nearby diffuse emission.
- PSRJ1112-6103: Very close to MSH 11 62 (arXiv:1202.3371v1). Nearby source is 2FGL J1112.1-6040. Significant extension.
- When fitting PSRJ1119-6127, description of adding nearby point source to represent emission residual from o represent residual from PSRJ1112-6103 looking spatially extended.
- PSRJ1418-6058 and PSRJ1420-6048, very difficult to analyze because both very near each other.
- Something about the complicated Gamma Cygni PSR: PSRJ2021+4026
- PSRJ1105-6107: something about adding source to background model that is very nearby.
- PSRJ1648-4611 (what to do about nearby 2FGL source and other residual emission. Is this paper relevant: http://arxiv.org/pdf/1111.2043.pdf???)?
- What to do about emission from PSR J1023 at low energy???
- PSRJ0908-4913: what to say about far localization?

1.4. Discussion

Maybe a pulsar physics person can fill in this section???

REFERENCES

Abdo, A. A., et al. 2010a, ApJS, 188, 405

—. 2010b, ApJ, 708, 1254

—. 2011, Science, 331, 739

Ackermann, M., et al. 2011, ApJ, 726, 35

Ackermann, M., et al. 2011, ApJ, 726, 35

Buehler, R., et al. 2012, ApJ, 749, 26

Grondin, M.-H., et al. 2011, ApJ, 738, 42

Jackson, B., et al. 2005, IEEE, Signal Processing Letters, 12, 105

Lande, J., et al. 2012, ApJ, in preparation

Nolan, P. L., et al. 2012, ApJS, 199, 31

A. Description of Auxiliary information for Off-peak Analysis

A more complete list of the results from the pipeline are contained in a supplimental `fits`-format table.

Here, we describe each column contained in the fits table:

- Column `TS_point` is the test statistic obtained at the best fit position of the assumed point-like source
- Column